Research article

Analysis of the pharmacokinetics and efficacy of RBD1016 – A GalNAc-siRNA targeting Hepatitis B Virus X gene using semi-mechanistic PK/PD model

Qian Li [a,1], Taohua Geng [b,1], Haiyan Li [b], Shuquan Zheng [b], Sara Svedlund [c], Liming Gan [b,c], Ann-Charlotte Egnell [b,c], Shan Gao [b,**], Rui Chen [a,***], Pei Hu [a,*]

[a] Clinical Pharmacology Research Center, Peking Union Medical College Hospital, State Key Laboratory of Complex Severe and Rare Diseases, NMPA Key Laboratory for Clinical Research and Evaluation of Drug, Beijing Key Laboratory of Clinical PK & PD Investigation for Innovative Drugs, Chinese Academy of Medical Sciences and Peking Union Medical College, Beijing, China
[b] Suzhou Ribo Life Science Co. Ltd., Jiangsu, 215300, China
[c] Ribocure Pharmaceuticals AB, Medicinaregatan 8A, Gothenburg, Sweden

ARTICLE INFO

ABSTRACT

Small interference RNA (siRNA) is a class of short double-stranded RNA molecules that cause mRNA degradation through an RNA interference mechanism and is a promising therapeutic modality. RBD1016 is a siRNA drug in clinical development for the treatment of chronic Hepatitis B Virus (HBV) infection, which contains a conjugated with N-acetylglucosamine moiety that can facilitate its hepatic delivery. We aimed to construct a semi-mechanistic model of RBD1016 in pre-clinical animals, to elucidate the pharmacokinetic/pharmacodynamic (PK/PD) profiles in mice and PK profiles in monkeys, which can lay the foundation for potential future translation of RBD1016 PK and PD from the pre-clinical stage to the clinic stage. The proposed semi-mechanistic PK/PD model fitted PK and PD data in HBV transgenic mice well and described plasma and liver concentrations in the monkeys well. The simulation results showed that our model has a reasonable predictive ability for Hepatitis B surface antigen (HBsAg) levels after multiple dosing in mice. Further PK and PD data for RBD1016, including clinical data, will assist in refining the model presented here. Our current effort focused on model building for RBD1016, we anticipate that the model could apply to other GalNAc-siRNA drugs.

1. Introduction

Small interference RNA (siRNA) is a class of short (21–25 nts) double-stranded RNA molecules that cause mRNA degradation through an RNA interference (RNAi) mechanism and thereby preventing translation to protein [1]. RNAi is an evolutionarily conserved mechanism of gene regulation found in various organisms [2,3], the endogenous siRNA can reduce gene expression through enzymatic cleavage of a target mRNA, or hindrance of translation, mediated by the RNA-induced silencing complex (RISC) [4]. In

---

principle, siRNA can target any mRNA, especially to treat genetic diseases currently untreatable by conventional medicine, thus offering a promising therapeutic modality.

The site of action of siRNA is the cytosol, and they must pass through a series of biological barriers from the administration site to reach the target site [4], a variety of potential delivery strategies are needed to overcome the problem [5]. The development of N-acetylgalactosamine (GalNAc) conjugates, which bind to the asialoglycoprotein receptor (ASGR) abundantly expressed on the surface of hepatocytes, has become a breakthrough approach for targeted delivery of siRNA to hepatocytes [6]. So far, GalNAc based therapies have held a prominent position in the drug development pipeline of several pharmaceutical companies [6], five GalNAc-based siRNA drugs have been approved by FDA, in which siRNAs are all conjugated to a GalNAc ligand and enable ASGPR - mediated targeted delivery to hepatocytes [7–9]. GalNAc is relatively simple to synthesize and can be administrated subcutaneously, and has shown favorable biocompatibility/toxicity profiles, as well as very high efficacy, so it is currently the most popular platform for siRNA delivery [10]. At present, most siRNA drugs in clinical trials are based on GalNAc conjugation [10,11].

RBD1016 is a GalNAc-siRNA drug in clinical development for treating chronic Hepatitis B Virus (HBV) infection [12]. Worldwide, more than 350 million people are infected with HBV [13], current treatments for HBV include nucleoside analogs and interferon-alpha administration, which have low efficacy on HBsAg reduction and undesirable side effects, thus new therapies that target multiple aspects of the HBV viral life cycle are needed [14]. The HBV genome contains four overlapping open reading frames that encode the different viral proteins. Due to its unique transcript arrangement and the fact that replication occurs via an RNA intermediate, RNAi therapy is an appealing treatment method [15]. RBD1016 is designed to target the highly conserved region of the HBV X-gene and can silence four HBV gene transcripts by RNAi, thus can simultaneously inhibit HBV DNA, HBsAg, and HBeAg expression.

There is no siRNA drug approved for treatment of HBV infection so far. Several siRNA drugs are currently being evaluated in preclinical and clinical trials. ARC-520 was the first-in-class siRNA for chronic HBV [16]. But the development of ARC-520 was terminated due to mortality induced by the excipient of ARC-520 (not the active siRNA component) in non-human primates. Following ARC-520, a series of novel siRNA drugs with indications for HBV infection have entered clinical trials, such as the GalNAc-conjugated siRNA drugs AB-729, RG-6346, VIR-2218 and JNJ-3989 [17]. Although much knowledge has been gained over the last decade about GalNAc-conjugated siRNAs, there is a lack of published literature on the pharmacokinetic (PK) and HBsAg inhibition efficacy of siRNA drugs for HBV, except for the two studies of ARC-520 [18,19] and two studies of JNJ-3989 [12,20] published recently.

Mechanism-based PK/PD models can integrate data from in vitro and *in vivo* studies as well as literature-derived values and can be used to extrapolate drug exposure and therapeutic effects, which is anticipated to reduce experimental attrition and facilitate the translation of complex therapeutics [21,22]. Several modeling efforts have also emerged to support the clinical development of siRNAs and regulatory submissions [23]. In terms of modeling applications for the clinical translation of experimental animal data of GalNAc-conjugated siRNA drugs, these include one minimal physiologically based pharmacokinetic-pharmacodynamic (mPBPK-PD) model [24] and a JNJ-3989 PK model in mice have been reported [12]. Developing mechanism-based PK/PD model for GalNAc-siRNA drugs can be resource-intensive, as the complexity of siRNA targeting to the liver, intracellular kinetic processes, and RNA interference in hepatocytes [1]. The mechanism-based model requires 30 or more parameters for its implementation, and many are difficult to obtain through in vitro experimental methods [24]. Traditional empirical models fail to integrate the mechanisms of GalNAc-siRNA targeting hepatocyte [25]. More examples and attempts at describing PK/PD modelling of GalNAc conjugated siRNA drugs are needed. Compared to mechanistic models, semi-mechanistic models can simplify the structure and parameters and include important mechanistic processes, which can help assist in GalNAc-siRNA drug development.

Therefore, we aimed to construct a semi-mechanistic model of RDB1016 in pre-clinical animals, to help us to understand the PK profiles of RDB1016 in HBV transgenic mice and healthy cynomolgus monkeys, and the PD profiles including inhibition efficacy for target mRNA and HBsAg in HBV transgenic mice. The model may also provide rational preclinical platforms to analyze exposure-efficacy relationships and to facilitate translation to the clinic.

2. Materials and methods

2.1. PK and HBsAg data collection

The RBD1016 liver concentration data, mRNA, and HBsAg data used for mice PK/PD model building were obtained from two studies in HBV transgenic mice (C57B/6N-Tg (1.28HBV)/Vst), one was single-dose PK-PD study, another was a single-dose PD study. The RBD1016 plasma concentration data were collected from a separate plasma PK study in HBV transgenic mice. All animal procedures were approved by the local Scientific Ethical Committee for Animal Testing.

In the HBV transgenic mice single-dose PK-PD study, the relationship between liver PK and PD biomarkers was investigated. Twenty-one mice were randomly divided into seven groups, with three mice in each group; one group was subcutaneously (SC) administered phosphate buffer saline (PBS) as vehicle control; the other six groups were administered RBD1016 (3 mg/kg, SC). The first day of dosing was designated Day1 (D1), and the 6 groups of mice which received RBD1016 were sacrificed at 6 predetermined time points after administration (D2, D8, D15, D29, D57, D85). The levels of HBsAg in serum, as well as HBV mRNA and total drug concentration in liver tissue were detected after terminal sampling of all animals. The dose level and time points selected in the single-dose PK/PD study were based on our previous experience.

In the HBV transgenic mice single-dose PD study, the dose-effect relationship was evaluated. Forty-eight mice were divided into six groups (eight mice per group), half male and half female. And each mice was subcutaneously injected with PBS or five different doses of RBD1016 (0.1, 0.3, 1, 3, and 9 mg/kg). Blood samples were collected at pre-dose and once weekly for the first 4 weeks post-dose and every two weeks thereafter. until day 85, and the samples were used for the analysis of HBsAg level.

In the separate plasma PK study, transgenic mice were administered 3 mg/kg RBD1016 or PBS subcutaneously to assess plasma PK characteristics. Blood samples were collected at 0.25, 0.5, 1, 2, 4, 6, and 10 h after administration, and the concentration was based on data from one individual animal for each timepoint.

The data used for the monkey plasma and liver PK model were obtained from a single-dose PK study in healthy cynomolgus monkeys. The SC dosing groups in this study contained twelve cynomolgus monkeys (half male and half female), animals were randomly assigned to 3 groups with 4 animals per group, and each group received a single subcutaneous injection of RBD1016 at a dose of 1, 3, or 9 mg/kg. Serial blood samples were collected at pre-dose and 10min, 30min, 1, 2, 4, 6, 8, 10, 24, 48, 96 h, and 7, 14, 21, 28, 35, 42, 56, 84, 112, 140 and 168 days post-dose. Liver samples were acquired by repeated ultrasound-guided percutaneous needle biopsy of the liver at time points 2, 14, 28, 56, 84, 112, 140, and 168 days post-dose (the first day of dosing day 1). A summary of information about the data used for model building can be found in Table S1.

2.2. Bioanalysis methods

RBD1016 consist of 19- to 23-nucleotide double-stranded RNA duplexes, one strand is the sense strand (RBD1016_SS), and the other strand is the antisense strand (RBD1016_AS). RBD1016_AS is a pharmacologically active component. RBD1016_AS has 2-nucleotide overhang at the 3′end, which can be degraded by nucleic acid into RBD1016_AS-3-1 and RBD1016_AS-3-2. In vitro studies showed that the activity of the metabolites (RBD1016_AS-3-1 and RBD1016_AS-3-2) was comparable to that of the original drug (RBD1016_AS). So, the concentration of RBD1016 was taken as the sum of the RBD1016_AS and the metabolite (RBD1016_AS-3-1 and RBD1016_AS-3-2) in our study.

The RBD1016 concentrations (include RBD1016_AS, RBD1016_AS-3-1 and RBD1016_AS-3-2) in blood samples were analyzed using a hybridization-based liquid chromatography-fluorescence assay. The lower limit of quantification (LLOQ) for the plasma assay was 0.729 ng/ml, and the linear calibration range was 0.729–364 ng/ml. The RBD1016 concentrations in mice liver samples were analyzed using high-performance liquid chromatography (HPLC) -high resolution mass spectrometry (HRMS), the LLOQ was 0.182 μg/g, and the linear calibration range was 0.182–364 μg/g. Monkey liver samples were analyzed using HPLC- fluorescence method with the linear calibration range 0.117–58.4 μg/g. Real-time quantitative PCR was performed to evaluate the HBV X-gene mRNA expression in the liver. Relative quantification was achieved using the comparative 2-ΔΔCt method; all samples were run in triplicate and normalized to GAPDH. HBsAg levels in blood samples were quantified using the chemiluminescence method, and the linear range was between 0.03 and 250 IU/mL. When building the PK model, liver concentrations expressed in ug/g were scaled to nmol/g based on the molecular weight of RBD1016 (MW was 15479.38 Da).

2.3. Semi-mechanistic PK/PD model

The PK and PD data (including liver HBV X-gene mRNA and serum HBsAg level) from HBV transgenic mice were used to build the mice semi-mechanistic PK/PD model, and a sequential PK–PD modeling approach was employed. The PK data from healthy cynomolgus monkeys were used to build the monkey semi-mechanistic PK model. The semi-mechanistic PK/PD model structure of
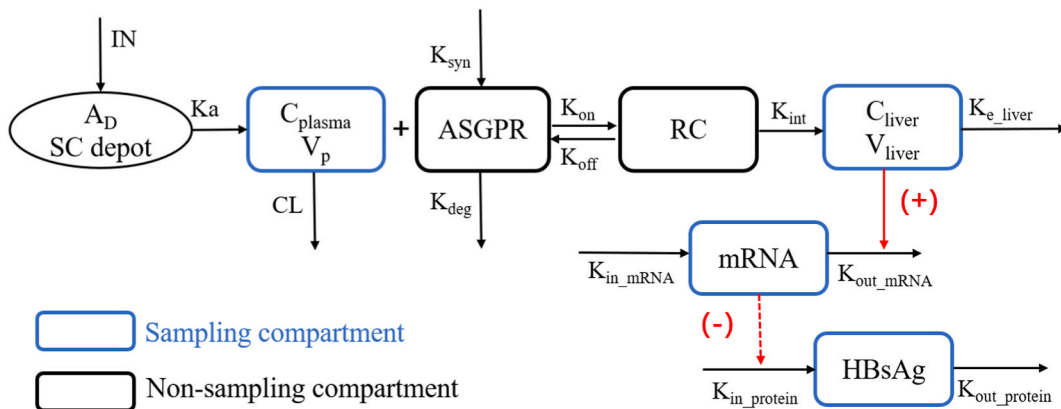

Fig. 1. Representation of the semi-mechanistic PK/PD model of RBD1016. A_D represents RBD1016 amounts in the absorption depot. C_{plasma} and C_{liver} represent the RBD1016 concentrations in plasma and liver, respectively. IN represents subcutaneously dosing, Ka represents the SC absorption rate constant, CL represents plasma clearance, K_{syn} represents the zero-order synthesis rate of the receptor (ASGPR), and K_{deg} represents the first-order degradation rate constant of ASGPR. K_{on} represents the association rate constant for GalNAc to ASGPR; K_{off} represents the dissociation rate constant for GalNAc to ASGPR. RC represents the ASGPR-GalNAc-siRNA complex. K_{int} represents the internalization rate constant for bound ASGPR, and K_{e_liver} represents the degradation rate constant for RBD1016 in the liver. K_{in_mRNA} represents the zero-order synthesis rate of target mRNA, K_{out_mRNA} represents the first-order degradation rate constant of target mRNA, $K_{in\_protein}$ represents the zero-order synthesis rate of HBsAg, $K_{out\_protein}$ represents the first-order degradation rate constant of HBsAg. Compartments in blue represent sampling compartments. Red solid line arrows represents stimulation of mRNA degradation; red dashed arrows indicate inhibition of HBsAg synthesis. (For interpretation of the references to colour in this figure legend, the reader is referred to the Web version of this article.)

RBD1016 is presented in Fig. 1. The PK part of the model was the same between mice and monkeys. Nonlinear mixed-effect modeling (Phoenix NLME version 8.3.1; Certara USA, Inc.) was performed for all analyses, and the first-order conditional estimation–extended least squares (FOCE-ELS) method was used for model building. Since the liver concentration of RBD1016 in mice and mRNA level were conducted with a destructive sampling approach (sacrificed at each time point), a naïve pooled approach was utilized when building the mice semi-mechanistic PK model.

A one-compartment model for plasma with an additional liver compartment, including binding to ASGPR and uptake from plasma to the liver compartment via ASPGR, was selected to describe RBD1016 PK. In this model, after SC dosing, a linear absorption for RBD1016 was characterized by Equation (1):

$$\frac{dA_D}{dt} = -Ka \times A_D \times F \hspace{4cm} \text{Equation 1}$$

where A_D represented the amounts of RBD1016 in the absorption compartment after SC administration, Ka represented the first-order absorption rate constant from the absorption compartment to the central compartment, F represented the bioavailability.

After SC absorption, the plasma concentration of RBD1016 was presented in the central compartment, with a central volume of distribution (V_p). The plasma concentrations (C_{plasma}) of RBD1016 in the central compartment were eliminated via a linear pathway, quantified by plasma elimination clearances (CL) or by binding to the ASGPR transporter (R). In the model, plasma RBD1016 binds to ASGPR, forming the ASGPR-GalNAc-siRNA complex (RC) according to the second-order association rate (K_{on}) and first-order dissociation rate constant (K_{off}) as described in Equation (2).

$$\frac{dCplasma}{dt} = \frac{A_D \times Ka \times F}{V_p} - \frac{CL \times C_{plasma}}{V_p} - K_{on} \times C_{plasma} \times R + K_{off} \times RC \hspace{2cm} \text{Equation 2}$$

Once the RC is formed, it is internalized into the hepatocytes, following a first-order process. The concentration of ASGPR (R) and RC were described in Equation (3) and Equation (4) separately.

$$\frac{dR}{dt} = K_{syn} - K_{deg} \times R - K_{on} \times C_{plasma} + K_{off} \times RC \hspace{3cm} \text{Equation 3}$$

$$\frac{dRC}{dt} = K_{on} \times C_{plasma} - K_{off} \times RC - K_{int} \times RC \hspace{3cm} \text{Equation 4}$$

Where K_{syn} and K_{deg} represent the biosynthesis and degradation rates of ASGPR. The initial value of mice liver ASGPR (R0) concentration was assumed to be 647 nM, as reported by Bon et al. [24,26], and was fixed in the model. K_{syn} derives from K_{deg} and R0, as $K_{syn} = K_{deg} \times R0$, and K_{int} represents the hepatocytes internalization rate constant for bound ASGPR.

After hepatocytes internalization, liver disposition was characterized by Equation (5), in which K_{e_liver} represented the first-order liver elimination rate.

$$\frac{dC_{liver}}{dt} = \frac{Kint \times RC \times V_p}{V_{liver}} - K_{e\_liver} \times C_{liver} \hspace{3cm} \text{Equation 5}$$

The dynamics of target mRNA and HBsAg were then described using an indirect response model with zero-order synthesis rate constants. In the model, RBD1016 in the liver compartment promotes the degradation of target mRNA (K_{out_mRNA}), and this will reduce the production of HBsAg (K_{in_HBsAg}) as described in Equations (6) and (7).

$$\frac{dmRNA}{dt} = K_{in\_mRNA} - K_{out\_mRNA} \times \left(1 + \frac{S_{max\_mRNA} \times C_{liver}}{C_{liver} + SC_{50}}\right) \times mRNA \hspace{2cm} \text{Equation 6}$$

$$\frac{dHBsAg}{dt} = K_{in\_HBsAg} \times \left(\frac{mRNA}{mRNA_0}\right)^{\beta} - K_{out\_HBsAg} \times HBsAg \hspace{2cm} \text{Equation 7}$$

where mRNA represented the level of mRNA, S_{max_mRNA} represented the maximum effect of RBD1016, C_{liver} represented the RBD1016 concentration in the liver, and SC_{50} represented the concentration producing 50 % of maximal response. K_{in_mRNA} represented the production of mRNA derived from K_{out_mRNA} and baseline mRNA ($mRNA_0$), as $K_{in\_mRNA} = K_{out\_mRNA} \times mRNA_0$. HBsAg represented the level of serum HBsAg, and K_{in_HBsAg} represented the production of HBsAg, which derived from K_{out_HBsAg} and baseline HBsAg ($HBsAg_0$), as $K_{in\_HBsAg} = K_{out\_HBsAg} \times HBsAg_0$. The exponent β is the shape factor determining the response curve's steepness.

2.4. Statistical model

A statistical model is a model that characterizes the differences between the predictions of the model and the observed values. In the statistical model, we incorporated two levels of random variation: between-subject variability (BSV) and within-subject variability (WSV). BSV refers to the deviation of individual parameter values from the typical population estimate parameters, an exponential model was used to describe the BSV. The exponential model was described as $\theta_i = \theta \cdot \exp(\eta_i)$, where θ_i represented the parameter estimate for the i th individual, θ represented the typical population estimate parameters, and $\exp(\eta_i)$ was the inter-individual random deviation of θ_i from θ. η_i was assumed to be normally distributed with mean zero and variance of ω_i^2.

WSV refers to the differences between the observed and predicted values of individuals that are caused by unknown factors. It typically arises from errors in measurement, sampling, and analysis, and represents the unexplained portion of the between-subject variability in model parameters. The residual error model was used to describe the WSV. The residual error model was multiplicative with the proportional error model, which described as $C_{obs} = C_{pred} \cdot (1 + \varepsilon_1) + \varepsilon_2$. C_{obs} represented the observed values, C_{pred} represented the predicted values, ε represented the residual variation, and ε was assumed to be normally distributed with mean zero and variance of σ^2.

Because a naïve pooled approach was utilized when building the mice semi-mechanistic PK model in mice, thus, no BSV terms were estimated in the mice PK model, and all the variability was attributed to the unexplained residual variability.

2.5. Model simulation and evaluation

The mice's final semi-mechanistic PK/PD model, which was built with single-dose PK and PD data, was used to simulate the serum HBsAg levels in mice after multiple-dose administration of RBD1016. We used a Monte Carlo simulation approach. The model was run with 1000 Monte Carlo simulations using typical values and between-subject and within-subject variability estimated from the final PK/PD model. The simulation dose regimens were 3 mg/kg SC q4w and q8w with a total of 3 times. The HBsAg data from model simulations were compared to observations for external validation. Plasma or liver concentration data were not available for the external validation mice multiple dosing data set.

The monkey semi-mechanistic PK model was diagnosed with goodness-of-fit (GOF) plots. GOF plots were used to evaluate general parameter precision, including conditional weighted residuals (CWRES) versus time; CWRES versus population predicted concentration (PRED); observed concentration (DV) versus PRED; DV versus individual predicted concentration (IPRED).

3. Results

3.1. PK and PD properties of RBD1016

Before constructing the semi-mechanistic model, we first conducted an exploratory data analysis (EDA) on the PK and PD data to gain insight into the nature of the data and to guide the model construction process. In the separate plasma PK study, following 3 mg/kg SC administration of RBD1016, the plasma concentration reached a maximum of 40.1 nmol/L at 0.5 h post-dose, then decreased rapidly and was below the LLOQ (0.047 nmol/L) after 2 h. The maximal concentration in the liver was observed 24 h post-dose and decreased slowly, and the liver RBD1016 was still detectable up to day 85 (Fig. 2). The mean mRNA expression decreased after dosing and reached a nadir on Day 29. There was a delay between the maximum mRNA inhibition effect and the peak concentration in the liver (Fig. 3). The inhibition of HBsAg was dose-dependent. The level of HBsAg reduced to a minimum of 0.16 % relative to the baseline on Day 15 in 3 mg/kg dose level. The efficacy of HBsAg inhibition was still observed for up to 85 days (Fig. 4).

In the healthy cynomolgus monkeys PK study, after SC administration of 1, 3, and 9 mg/kg single doses, exposure to RBD1016 in plasma increased in a greater than dose-proportional manner. Consistent with potential saturation of ASGPR-mediated disposition, the greater than dose-proportional exposure in plasma was associated with a less than dose-proportional increase in liver exposure (data not shown).
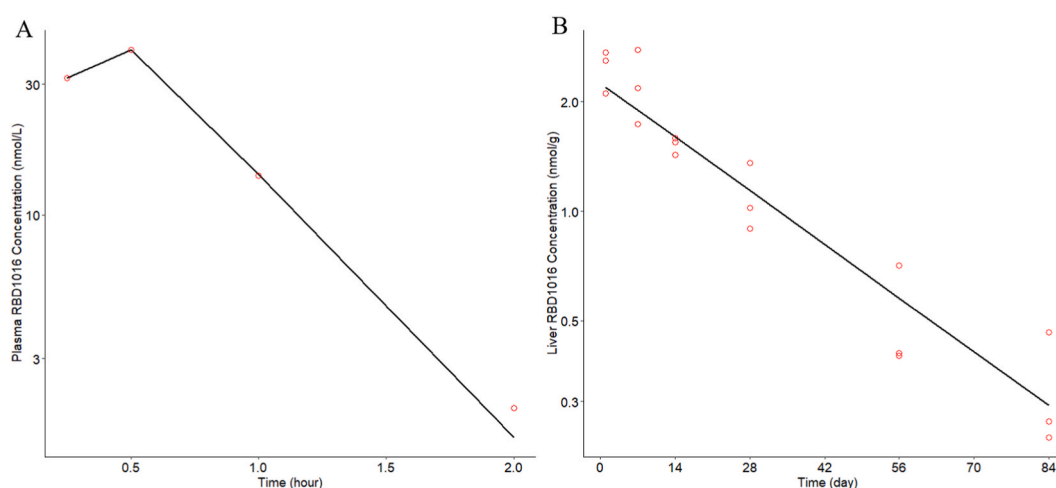

Fig. 2. Semi-mechanistic PK/PD model fittings in PK data. Plasma RBD1016 concentration versus time (A); Liver RBD1016 concentration versus time (B). Red circles represent the observed concentration, and lines represent model predictions. Plasma observations were collected from n = 1 mice for each time point, liver observations were collected from n = 3 mice for each time point after SC 3 mg/kg RBD1016. (For interpretation of the references to colour in this figure legend, the reader is referred to the Web version of this article.)

Fig. 3. Semi-mechanistic PK/PD model fitting in target mRNA levels. Red circles represent the observed mRNA, and black line represents model predictions. Liver mRNA observations were collected from n = 3 mice for each time point after SC 3 mg/kg RBD1016. (For interpretation of the references to colour in this figure legend, the reader is referred to the Web version of this article.)
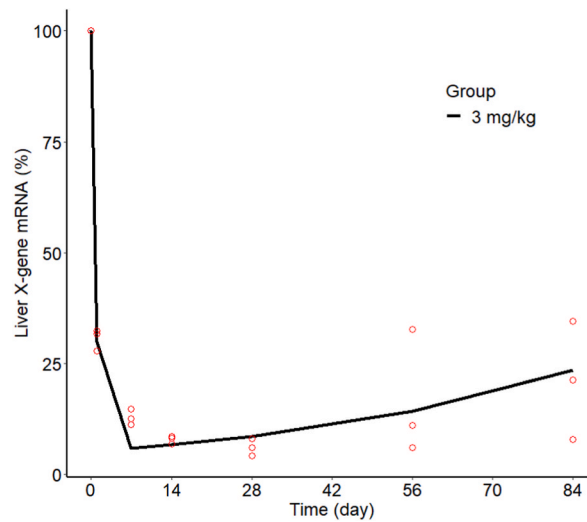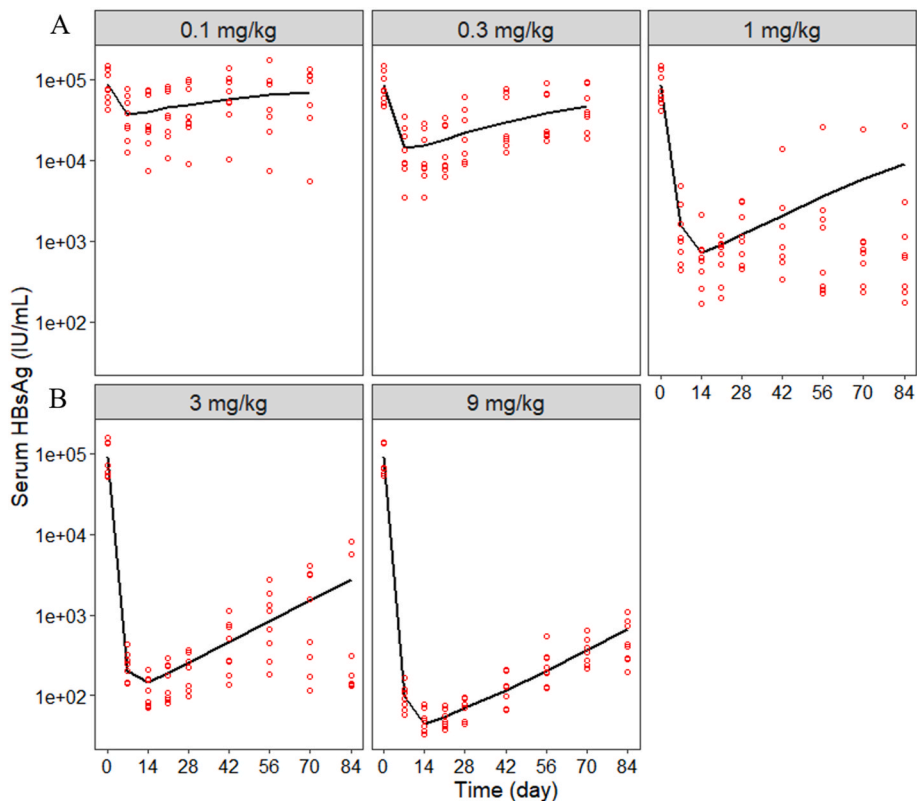

Fig. 4. Semi-mechanistic PK/PD model fitting in HBsAg expression levels. HBsAg expression level for the 0.1 mg/kg, 0.3 mg/kg, 1 mg/kg dose groups (A); HBsAg expression level for the 3 mg/kg and 9 mg/kg dose groups (B). The red circles on each plot represent the HBsAg observation for each of the five dose groups, and the black lines represent model predictions. Serum HBsAg observations were collected from n = 8 mice from each group. (For interpretation of the references to colour in this figure legend, the reader is referred to the Web version of this article.)

3.2. Mice semi-mechanistic PK/PD model

The mean plasma and liver PK data of RBD1016 and the mean expression level of mRNA and HBsAg per time point were used to construct the semi-mechanistic mice PK/PD model. Because the PK data and liver tissue mRNA levels from the HBV transgenic mice were conducted with a destructive sampling approach (one sample per mouse), a naïve pooled approach was utilized when estimating the parameters related to these data. The plasma concentration data and mean liver concentration data in the 3 mg/kg group were used to build the PK model, the mean mRNA expression data in the 3 mg/kg group, and HBsAg data in all single dose groups were used to construct the PD model.

Table 1 summarized the parameters estimated from the mice semi-mechanistic PK/PD model, the PK parameters were estimated with adequate precision as the relative standard error percent (RSE) was below 10 %, but the PD parameters K_{out_mRNA} and S_{max_mRNA} had larger RSE (96.3 % and 117 %, respectively). The absorption rate constant (Ka) after SC administration was 2.1 h^{-1}, plasma RBD1016 clearance was 0.09 L/h, and the estimated central volume of distribution was 0.00267 L RBD1016 rapidly accumulated in the liver through ASGPR-mediated endocytosis after absorption, the K_{on} was 0.53 $nM^{-1} \cdot h^{-1}$, K_{off} was 1.32 h^{-1}, they were fixed to literature value [24]. The liver half-life was 28.9 days (0.693/K_{e_liver}), substantially longer than the plasma half-life.

Fig. 2 depicts the time course of observed versus model-predicted PK data in HBV transgenic mice. The proposed semi-mechanistic PK/PD model captured the concentration-time profiles of RBD1016 both in plasma (Fig. 2A) and liver (Fig. 2B). Figs. 3 and 4 depicts the time course of observed versus model-predicted PD data in HBV transgenic mice, including target mRNA (Fig. 3) and HBsAg expression level (Fig. 4). In which, Fig. 4A shows the observed and predicted HBsAg expression level for the 0.1–1 mg/kg dose groups, and Fig. 4B shows the observed and predicted HBsAg expression level for the 3–9 mg/kg dose groups.

3.3. Monkey semi-mechanistic PK model

A total of 190 concentration data, including plasma and liver concentrations from 1, 3, and 9 mg/kg dose groups were used to build the monkey semi-mechanistic PK model. The final semi-mechanistic PK model parameter estimates were summarized in Table 1. All the parameters were estimated with adequate precision as RSE was below 30 %. The absorption rate constant after SC administration was 0.315 h^{-1}, plasma clearance was 1.89 L/h, and the estimated central volume of distribution was 2.33 L. ASGPR receptor and its degradation rate constant (K_{deg}) were physiologically related parameters, they were fixed as the values reported in the literature [24]. The values of K_{on} and K_{off} have not been reported in cynomolgus monkeys. If the two parameters were assumed to be the same as those in mice, the model cannot fit the data well. Therefore, K_{on} and K_{off} of cynomolgus monkeys were estimated in our model, and K_{on} was 0.004 $nM^{-1} \cdot h^{-1}$, and K_{off} was 1.56 h^{-1}. The liver RBD1016 half-life was 32.1 days (0.693/K_{e_liver}), substantially longer than the plasma half-life. The model fitting results for individual plasma and liver RBD1016 concentrations were shown in Figs. 5 and 6, respectively. Our results showed that the model fitted the monkey plasma and liver drug concentration data well.

3.4. Model simulation and evaluation

The simulation results suggested that the mouse PK/PD model had a reasonable predictive ability for HBsAg levels in HBV transgenic mice after multiple doses of RBD1016 (Fig. 7). For group 3 mg/kg SC q4w, the observed values were mostly within the 90 % confidence intervals of the forecasted values (Fig. 7A). For group 3 mg/kg SC q8w, the predicted HBsAg levels were consistent with the overall variation trend of the observations, but the model underpredicted the inhibition of HBsAg expression after the first dose (Fig. 7B). We acknowledge it as the limitation of our model because plasma and liver concentrations were not collected for the multiple-dose PD study, hence, we could not determine whether this prediction bias originates from the PK or PD part of the semi-

Table 1
Semi-mechanistic PK/PD model parameter values in mice and monkey.

Parameter	Unit	Description	Mice Estimate (RSE%)	Monkey Estimate (RSE%)
V	L	Central volume of distribution	0.00267 (1.6)	2.33 (11.7)
V_{liver}	g	Liver weight	0.8 (Fixed) [11]	63 (Fixed) [27]
Ka	1/h	Subcutaneous absorption rate constant	2.10 (1.5)	0.315 (9.9)
CL	L/h	Plasma RBD1016 clearance	0.09 (0.5)	1.89 (9.0)
K_{on}	1/(nM*h)	Association rate constant for GalNAc to ASGPR	0.53 (Fixed) [23]	0.004 (21.4)
K_{off}	1/h	Dissociation rate constant for GalNAc to ASGPR	1.32 (Fixed) [24]	1.56 (14.5)
K_{deg}	1/h	Degradation rate constant for ASGPR	0.044 (Fixed) [26]	0.044 (Fixed) [26]
K_{int}	1/h	Internalization rate constant for bound ASGPR	2.4 (Fixed) [24]	0.137 (16.6)
K_{e_liver}	1/h	Degradation rate constant for RBD1016 in liver	0.00101 (4.7)	0.0009 (16.6)
R0	nM	Baseline ASGPR density in hepatocytes	647 (Fixed) [26]	339 (Fixed) [24]
K_{out_mRNA}	1/h	Degradation rate constant for target mRNA	0.0129 (96.3)	NA
S_{max_mRNA}	NA	Maximal stimulation of target mRNA degradation	65.6 (117)	NA
SC_{50_Cliver}	nM	Liver concentration at half-maximal effect	6.62 (58.7)	NA
mRNA0	%	Baseline mRNA in mouse liver	100 (Fixed)	NA
K_{out_HBsAg}	1/h	Degradation rate constant for HBsAg	0.0431 (26.6)	NA
β	NA	Beta coefficient for protein translation	2.29 (23.8)	NA

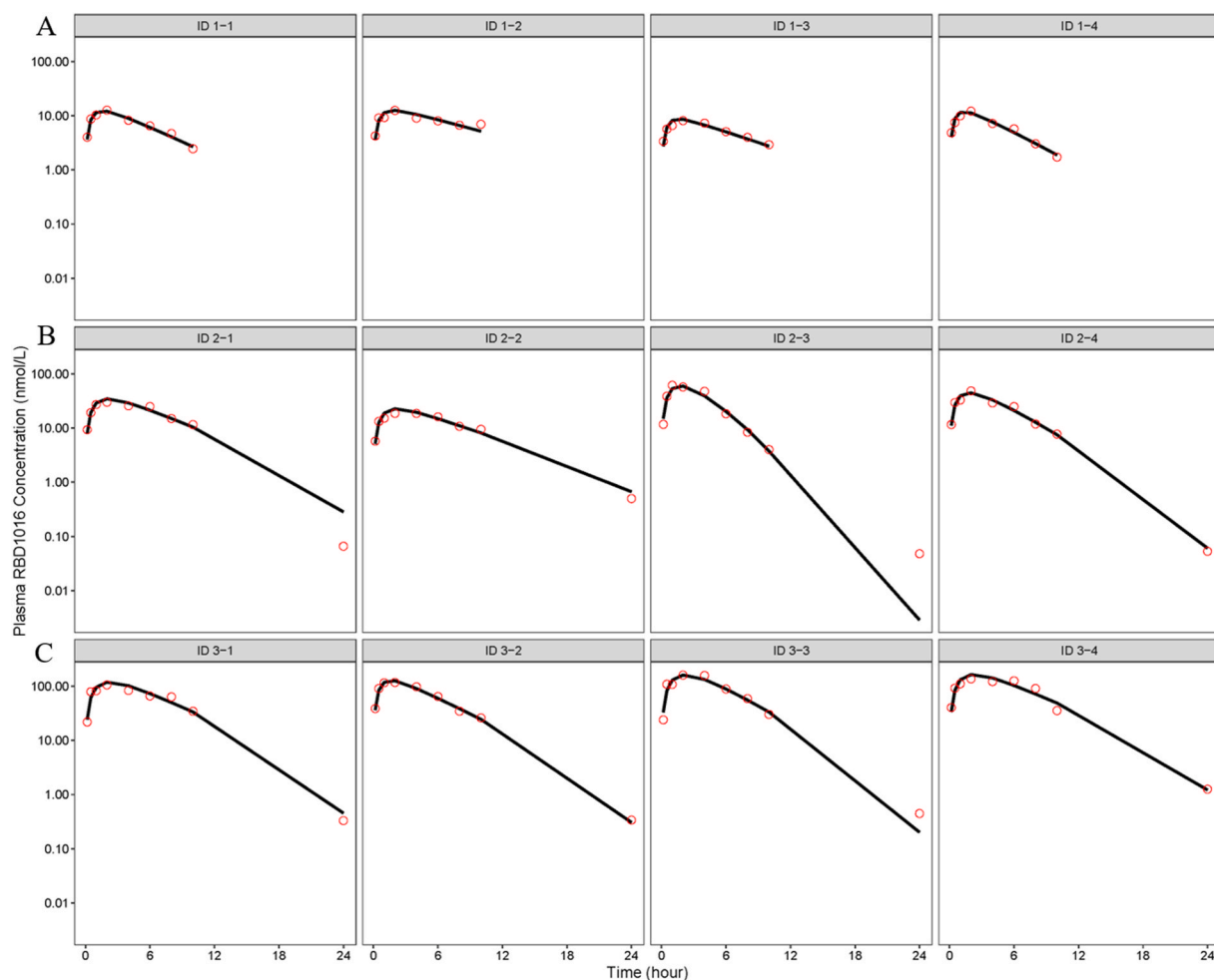RSE, relative standard error; NA, not applicable.

Fig. 5. Monkey semi-mechanistic PK model fittings in individual plasma RBD1016 concentration. Red circles represent plasma RBD1016 concentration for each individual, and black lines represent model predictions. The first row in the figure shows data from 1 mg/kg dose group (A); the middle row was data from 3 mg/kg dose group (B); the bottom row was data from 9 mg/kg dose group (C). (For interpretation of the references to colour in this figure legend, the reader is referred to the Web version of this article.)

mechanistic model, or because of variation between these two dose regimen studies in the observed values.

The goodness-of-fit (GOF) plots for the monkey semi-mechanistic PK model were provided in Fig. S1 to Fig. S2. The conditional weighted residuals (CWRES) vs. time or vs. individual-predicted (IPRED) showed that most CWRES were within the range of $(-2, 2)$. The population-predicted (PRED) and IPRED plasma and liver RBD1016 concentrations vs. observed concentrations showed no major bias. These model diagnostics suggested that the semi-mechanistic PK model of the monkey adequately describes the plasma and liver RBD1016 concentrations.

4. Discussion

Small interfering RNAs (siRNAs) have emerged as an exciting strategy for gene therapy in treating human diseases by silencing harmful genes [28]. Duplex siRNAs cannot easily penetrate hydrophobic cellular membranes without assisting carriers, so cell-specific targeted delivery of siRNAs *in vivo* is perhaps the most critical consideration in developing an effective RNAi-based therapeutic agent [29]. One of the most successful conjugation delivery systems is the GalNAc platform which efficiently and specifically delivers siRNAs to liver hepatocytes that express high levels of ASGPR, the high-affinity receptor for GalNAc [30]. The model-based drug development can be applied to streamline the overall drug discovery, including development and regulatory evaluation processes [31]. In our study, semi-mechanistic PK and PK/PD models for RBD1016 - a GalNAc-siRNA intended for HBV infection, were developed using data collected from pre-clinical studies. The developed pre-clinical models characterized the PK and PD data of RBD1016 in mice and PK profiles in monkeys, and were able to reasonably predict HBsAg expression in mice following multiple doses of SC administration of RBD1016. To the best of our knowledge, this study reports the first semi-mechanistic PK/PD model of GalNAc-siRNA in HBV mice and the first semi-mechanistic PK model of GalNAc-siRNA in monkeys, we anticipate that the model could contribute to our further clinical
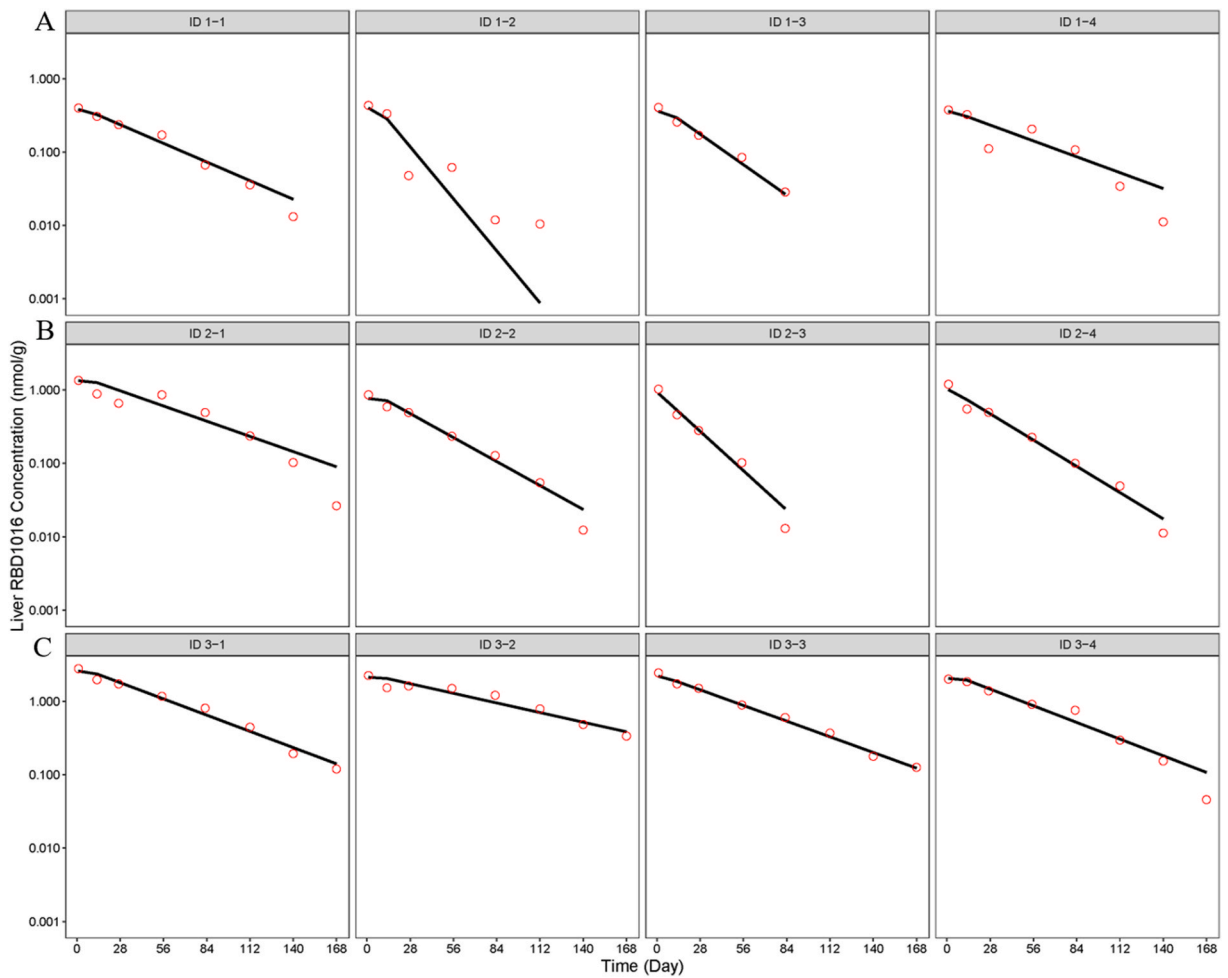
Fig. 6. Monkey semi-mechanistic PK model fitting in individual liver RBD1016 concentration. Red circles represent liver RBD1016 concentration for each individual, and black lines represent model predictions. The first row in the figure shows data from 1 mg/kg dose group (A); the middle row was data from 3 mg/kg dose group (B); the bottom row was data from 9 mg/kg dose group (C). (For interpretation of the references to colour in this figure legend, the reader is referred to the Web version of this article.)
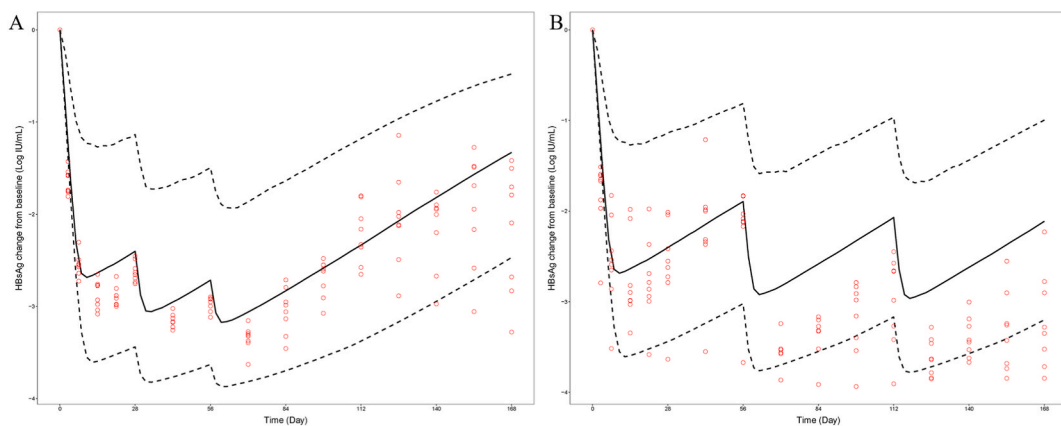

Fig. 7. Simulation results of the semi-mechanistic PK/PD model. The red circles on each plot indicate the HBsAg observation in group 3 mg/kg SC q4w (A) or q8w (B) with a total of 3 times in the multiple-dose PD study. Black solid lines represent model predictions of median HBsAg following 3 mg/kg SC q4w*3 (A) or q8w*3 (B). Dashed lines denote upper and lower 90 % confidence intervals. (For interpretation of the references to colour in this figure legend, the reader is referred to the Web version of this article.)

study of RBD1016.

GalNAc-siRNA exhibited unique pharmacokinetic and pharmacodynamic characteristics. GalNAc residues is one of the specific ligands for ASGPR expressed on the surface of hepatocytes. GalNAc-siRNA, through its conjugated GalNAc ligand, allows rapid and targeted delivery of siRNAs to hepatocytes. The plasma concentrations of GalNAc-siRNA are transient, the rapid clearance of GalNAc-siRNAs from the blood is consistent with rapid distribution to the hepatic tissue by receptor-mediated uptake through ASGPR [30], and the low molecular weight (~13 kDa) and small size (~7 nm) facilitating glomerular filtration (pore size ~8 nm) [32]. The onset of action is typically delayed relative to the time of administration, and the pharmacological effects last for a long time [33,34]. For GalNAc-siRNA, the concentration in the liver directly related to the gene silencing effect, one of the critical aspects of GalNAc- siRNAs development is the knowledge of kinetics in liver tissue. In a recent study by Nair et al. [35], they compared the PK and transthyretin (Ttr) mRNA knockdown activity of two siRNAs in mice, which have the same sequence but different chemical modifications. Their results showed that both siRNAs had similar plasma PK properties but different knockdown activities due to different exposures in the liver, demonstrating that the effects of GalNAc-siRNA were correlated with liver concentrations. Christopher R. Brown et al. [33] investigated the possible mechanistic explanations for the extended duration of GalNAc–siRNA activity observed *in vivo*. Their results also indicated that there was a direct correlation between liver concentration and drug efficiency. The chemical stability of siRNA in acidic intracellular compartments (e.g., lysosomes) within hepatocytes was a significant driver of prolonged activity duration.

In our study, after subcutaneous injection of RBD1016 into transgenic mice and monkeys, the RBD1016 rapidly accumulated in hepatocytes and was slowly eliminated in liver tissue with a liver half-life of 29 days and 32 days, respectively. RBD1016 must pass through a series of biological barriers from the administration site to reach the target site, so the effect is delayed relative to the plasma concentration. The efficacy of RBD1016 (HBV mRNA expression) decreased after dosing and reached a nadir on Day 29, although peak plasma concentrations are reached after 0.5 h of dosing. And the inhibition efficacy was still observed for up to 85 days. Similar pharmacokinetic profiling was reported in JNJ-3989, which distributes from plasma to liver via ASGPR mediated liver internalization in less than 24 h, with sustained (>42 days) liver exposure after administered subcutaneously in mice [12]. The kinetics of ARC-520 has been reported by Trubetskoy VS et al. [16], different form RBD1016, ARC-520 was administered intravenously, but like RBD1016, total amount of guide strands observed in liver exceeded that observed in the other tissues, and has slower elimination rate in liver than in plasma.

HBV has a narrow host range, causing chronic infection only in humans and chimpanzees, but the use of chimpanzees is strongly restricted and not easily available for HBV research [36], so we used HBV transgenic mice to analyze the relationship between PK and PD. X gene mRNA was one of the indicators of PD that we collected, results showed there was a 2-week delay in the maximum inhibition of mRNA relative to the peak liver concentration of RBD1016 in mice. The inhibitory effect gradually decreases as the hepatic concentration of RBD1016 slowly decreases, and the therapeutic effect is maintained until 85 days after a single dose of 3 mg/kg. Because of this unique PK/PD characteristic of GalNAc–siRNA, it was necessary to use liver concentration to establish exposure-effect relationships of RBD1016.

There have been several computational models of GalNAc–siRNA in the literature, which was used both in pre-clinical and clinical settings for different applications in product development [23], but the modeling of siRNA therapeutics is still in its infancy. Vivaswath S. Ayyar et al. [24] developed a minimal physiologically based pharmacokinetic-pharmacodynamic (mPBPK-PD) model for GalNAc-siRNA to facilitate preclinical-to-clinical translation. This model required the input of up to 30 parameters, including ASGPR binding rates, endosomal escape rates, and the formation of RNA-induced silencing complex (RISC), which may be challenging to characterize experimentally. The complexity of the PBPK model and diverse choice of parameters have limited its further application. An empirical compartment-based modeling approach was used to describe the exposure-effect relationship in nonclinical animals and extrapolated to humans via allometric scaling based on body weight or liver weight [25]. However, these models did not integrate knowledge system-specific parameters related to ASGPR (e.g., receptors per cell, degradation half-life, and recycled fraction), which was very important for understanding *in vivo* biodistribution of GalNAc-siRNA. Here, according to the liver-targeted distribution characteristics of GalNAc-siRNA [37], we constructed a semi-mechanistic PK/PD model. The PK part of the model consists of plasma compartment and liver compartment, and the ASGPR receptor-mediated uptake process in hepatocytes was included in the model. RBD1016 in liver decreased by a first-order elimination rate constant.

ASGPR density (R) is very important for GalNAc-siRNA uptake into the liver. ASGPR saturation is generally associated with a less-than-dose-proportional increase in liver exposure and a greater-than-dose-proportional increase in plasma exposure [30]. The values of ASGPR density in mouse liver reported in the literature are consistent [26,38]. This parameter is species-specific, so we fixed it to a value from the literature (647 nM in mice, 340 nM in monkeys). However, the uptake through the ASGPR depends not only on the receptor numbers but also on the kinetics of the receptor, e.g., receptor turnover rate. Charlotte Bon et al. [26] reported that the degradation rate constant (K_{deg}) of ASGPR in mice was 0.04 h^{-1}; in our model, we assumed the value of K_{deg} was the same between mice and monkeys and fixed to 0.04 h^{-1}. GalNAc-siRNA could bind to free ASGPR to form a GalNAc-ASGPR complex through an association rate constant (K_{on}). Once the complex is formed, it could either dissociate (K_{off}) or be internalized (K_{int}). Vivaswath S. Ayyar reported K_{on}, K_{off}, and K_{int} were 0.53 $nM^{-1} \cdot h^{-1}$, 1.32 h^{-1}, and 2.4 h^{-1} in the mice PBPK model, respectively. The GalNAc and ASGPR binding affinity depends on the number of GalNAc clusters present in the molecule [39]. RBD1016 uses a triantennary GalNAc ligand that binds to the ASGPR with high affinity [40]; we assumed that nucleic acid sequence and species do not affect GalNAc and ASGPR binding kinetics, and we fixed these parameters to Vivaswath S. Ayyar [24] reported values in mice PK model. Currently, the values of K_{on} and K_{off} in monkeys have not been reported in the literature. In our model K_{on} estimated from monkeys is smaller than mice, so ASGPR affinity may vary between species. To our knowledge, there is no relevant literature reporting differences of GalNAc and ASGPR affinity between mouse and monkey. Thus, more data are needed to gain insight into different species variation in ASGPR affinity. Finally, the model fitted the liver PK profile in mice (Fig. 2) and cynomolgus monkeys well (Figs. 5–6).

The narrow host range of HBV infection provided an obstacle to the establishment of an animal model of HBV infection. Most advances in HBV research have been gained using mice models with HBV replication or infection. So, in our study, we obtained mRNA and HBsAg data from HBV transgenic mice (C57B/6N-Tg (1.28HBV)/Vst) and established the semi-mechanistic PK/PD model only in mice. For RBD1016, the maximum mRNA suppression observed in the transgenic mice occurred 15 days after administration and was significantly delayed relative to the peak hepatic concentration. The delay was a commonly acknowledged phenomenon in the siRNAs PK-PD relationship [33,35,41,42]. A series of processes lead to the delayed effect of siRNA, which is transported from the site of administration to the target tissue, taken up into the target cells, transported into the cell endosomes, escapes from the endosomes, forms the RISC complexes, and target proteins turnover time [33]. The literature about the GalNAc-siRNA PD model is generally sparse. Alessandro Boianelli et al. [42] and Vivaswath S. Ayyar et al. [24] used indirect effect models to describe changes in target mRNA or protein; modelling efforts for Patisiran, Givosiran, and Inclisiran also used a similar indirect effect model approach to support regulatory approval in FDA multi-discipline review. In our study, an indirect-response model was developed with an E_{max} effect model linking liver RBD1016 concentrations with mRNA level, and mRNA degradation lowering the level of the translated HBsAg. We are not aware of any published report of synthesis rate constants and degradation rate constants of HBV mRNA and HBsAg - this is the first time these parameters have been reported.

The mice model building uses mean data, because the small size of the mice was not suitable for the continuous collection of plasma samples, and mice need to be sacrificed to obtain liver tissue for measurement of RBD1016 concentration and mRNA level. The PK parameters in mice were well estimated with RSE below 30 %. The PD parameters K_{out_mRNA} and S_{max_mRNA} had larger RSE (96.3 % and 117 %, respectively), suggesting the limited data may be inadequate to accurately estimate these parameters. Simulation results showed the model performed well in predicting HBsAg 3 mg/kg SC q4w and the first dose of 3 mg/kg SC q8w, performed poorly in the second and third doses of 3 mg/kg SC q8w. This implies that the model may be effective at predicting one dosing regimen and not so good at predicting another. The model did not predict all multiple-dose regimens well, the exact cause of this is not yet known. The reasons may be the mice plasma and liver PK data and mRNA data used to establish the model were only available for a single dose of 3 mg/kg, and the accumulation pattern of drugs in the liver after multiple doses was not clear. In addition, the RSE of PD parameters are large, and the observed values of HBsAg with multiple doses are highly variable among individuals. This suggests that in the following study if we want to build a model that better describes the PK/PD relationship, it is necessary to collect plasma and liver drug concentrations and mRNA indicators in different dose groups and multiple doses. For the PK model in monkeys, blood samples were obtained consecutively, and liver samples were acquired by repeated ultrasound-guided percutaneous needle biopsy, allowing the use of individual data to build the model. The PK parameters were well estimated (RSE%<30 %) in the monkey. The model was evaluated using the goodness-of-fit plots (GOF) method.

Understanding how PK translates between species is pivotal to supporting the first-in-human dose selection from pre-clinical data [43], and experience in siRNA drug translation is limited. A recent study collected time-course biomarker data for 11 GalNAc–siRNAs in various species and applied the PK-PD modeling approach to estimate the biophase (liver) half-life and potency. Their analysis indicates that siRNAs are generally more potent in humans than in mouse and monkey and that liver half-life is in the range of 0.6–3 weeks in mouse, 1–8 weeks in monkey, and 1.5–14 weeks in human. This is largely consistent with our liver half-life estimates (4.1 and 4.6 weeks in mouse and monkey respectively) [42].

Also, if the model is used to predict human PK/PD in the future, we should translate the parameters from pre-clinical animals to humans. In our semi-mechanistic model, some parameters were physiologically relevant parameters, like ASGPR density (R0) and degradation rate constant for ASGPR (K_{deg}), which could be obtained from the literature, or if the literature has not yet been reported, experiments need to be designed to determine these parameters. Other parameters were drug-related, such as the hepatic clearance constant (K_{e_liver}). Extrapolation of drug-related parameters is limited by the scarcity of siRNA drugs currently on the market and limited data. More non-clinical and clinical data on different GalNAc-siRNAs need to be collected to explore how to extrapolate. For small molecule drugs and antibody drugs, interspecies allometric scaling using eg bodyweight, has been widely used in the prediction of pharmacokinetic parameters of a species of interest. The allometric relationship is based on the power-law function, which can be represented as $Y = a \times W^b$, where Y is the parameter of interest, W represents the average body weight of a species, and a and b are the allometric coefficient and exponent of the equation, respectively [44]. We explored the applicability of the allometric scaling method for PK parameter extrapolation between two species (mouse and monkey) of GalNAc-siRNA drugs. Results showed allometric exponents were different from the exponents of 1.0 for V and 0.75 for CL, which were widely used in small molecules and antibody drugs parameter extrapolation. Exploratory allometric scaling of our mouse and monkey K_a, and K_{e_liver} parameters showed that they decreased as expected from mouse to monkey, but also differs from the generally assumed −0.25 exponent for first-order rate constants.

However, our results were based only on data from mouse and monkey of RBD1016, there have been a lot of uncertainties about the capacity to extrapolate to human PK/PD profiles. The uncertainty arises from the fact that we still do not have an in-depth understanding of the kinetic processes after siRNA entry into hepatocytes, the kinetic processes of target mRNA degradation, and the turnover processes of target proteins in different species. And limited by the detection methods, there are challenges for the localization and quantification of siRNAs in the cell. In addition, a few GalNAc-siRNA drugs were approved for marketing, and relatively few publicly available data could be used to explore the extrapolation method. This study is focused on RBD1016, but we hope to apply the PK/PD model to other GalNAc-siRNA candidates. Several factors need to be considered when applying the modeling to different therapeutic candidates, for example, 1) different siRNA sequences and modifications, 2) ASGPR receptor abundance and affinity, 3) target mRNA and protein kinetics, 4) individual differences, disease states, and other factors on the model. So, large amount of non-clinical and clinical data needs to be accumulated if we hope to accurately extrapolate the PK/PD model from animals to humans.

The study had some limitations. The data used to build the mice PK/PD model was rather limited and only included one dose group,

which might explain the uncertainty associated with the estimation of e.g. parameters K_{out_mRNA} and S_{max_mRNA}. This also limited the possibility of characterizing the potential saturation of ASGPR at higher doses. Further dose regimen-finding studies are required to explore these PK/PD relationships. Multiple dosing studies including both plasma and liver PK, and a PD or response measure, were lacking, limiting the ability to characterize e.g. liver concentration accumulation and effects on mRNA levels and HBsAg. RBD1016 is currently being tested in phase I clinical trials, further work is warranted to optimize the model following clinical data collection.

In summary, our study constructed a semi-mechanistic PK/PD model of RBD1016 in mice and a PK model in monkeys; the model fitted PK and PD data in mice well and well-described plasma and liver concentrations in the monkeys. The simulation results showed that the mice PK/PD model has a reasonable predictive ability for HBsAg levels after multiple dosing in mice. The GOF plots of the monkey semi-mechanistic PK model suggested that this model adequately describes the plasma and liver RBD1016 concentrations in monkeys. The models could help us to understand the exposure-effect relationships of RBD1016 in nonclinical animals. With the subsequent collection of more non-clinical and clinical data of RBD1016, we will further optimize the PK/PD model. This study is expected to be useful for the model-informed drug development of GalNAc-siRNA drugs.

Funding

Data availability

The raw data supporting the conclusions of this article will be made available by correspondence authors, upon reasonable request.

CRediT authorship contribution statement

Qian Li: Writing – original draft, Software, Methodology. **Taohua Geng:** Writing – original draft, Software, Methodology. **Haiyan Li:** Supervision, Investigation, Data curation. **Shuquan Zheng:** Project administration, Investigation, Data curation. **Sara Svedlund:** Resources, Project administration, Investigation. **Liming Gan:** Validation, Supervision, Investigation. **Ann-Charlotte Egnell:** Writing – review & editing, Visualization, Validation, Conceptualization. **Shan Gao:** Writing – review & editing, Visualization, Resources, Conceptualization. **Rui Chen:** Writing – review & editing, Visualization, Validation, Funding acquisition, Conceptualization. **Pei Hu:** Writing – review & editing, Visualization, Supervision, Project administration, Funding acquisition, Conceptualization.

Declaration of competing interest

The authors declare that they have no known competing financial interests or personal relationships that could have appeared to influence the work reported in this paper.

Acknowledgements

Appendix A. Supplementary data

Supplementary data to this article can be found online at https://doi.org/10.1016/j.heliyon.2024.e31924.

References

[1] K. Deprey, N. Batistatou, J.A. Kritzer, A critical analysis of methods used to investigate the cellular uptake and subcellular localization of RNA therapeutics, Nucleic Acids Res. 48 (14) (2020) 7623–7639, https://doi.org/10.1093/nar/gkaa576.

[2] A. Fire, S. Xu, M.K. Montgomery, S.A. Kostas, S.E. Driver, C.C. Mello, Potent and specific genetic interference by double-stranded RNA in Caenorhabditis elegans, Nature 391 (6669) (1998) 806–811, https://doi.org/10.1038/35888.

[3] C.C. Mello, D. Conte Jr., Revealing the world of RNA interference, Nature 431 (7006) (2004) 338–342, https://doi.org/10.1038/nature02872.

[4] J.C. Burnett, J.J. Rossi, RNA-based therapeutics: current progress and future prospects, Chem. Biol. 19 (1) (2012) 60–71, https://doi.org/10.1016/j.chembiol.2011.12.008.

[5] M.M. Zhang, R. Bahal, T.P. Rasmussen, J.E. Manautou, X.B. Zhong, The growth of siRNA-based therapeutics: updated clinical studies, Biochem. Pharmacol. 189 (2021) 114432, https://doi.org/10.1016/j.bcp.2021.114432.

[6] H. Cui, X. Zhu, S. Li, P. Wang, J. Fang, Liver-targeted delivery of oligonucleotides with N-acetylgalactosamine conjugation, ACS Omega 6 (25) (2021 Jun 14) 16259–16265, https://doi.org/10.1021/acsomega.1c01755.

[7] P. Kumar, R. Degaonkar, D.C. Guenther, et al., Chimeric siRNAs with chemically modified pentofuranose and hexopyranose nucleotides: altritol-nucleotide (ANA) containing GalNAc-siRNA conjugates: in vitro and in vivo RNAi activity and resistance to 5'-exonuclease, Nucleic Acids Res. 48 (8) (2020) 4028–4040, https://doi.org/10.1093/nar/gkaa125.

[8] Y. Chen, S.H. Xiong, F. Li, et al., Delivery of therapeutic small interfering RNA: the current patent-based landscape, Mol. Ther. Nucleic Acids 29 (2022) 150–161, https://doi.org/10.1016/j.omtn.2022.06.011.

[9] S.J. Keam, Vutrisiran: first approval, Drugs 82 (13) (2022) 1419–1425, https://doi.org/10.1007/s40265-022-01765-5.

[10] M. Friedrich, A. Aigner, Therapeutic siRNA: state-of-the-art and future perspectives, BioDrugs 36 (5) (2022) 549–571, https://doi.org/10.1007/s40259-022-00549-3.

[11] A. Khvorova, J.K. Watts, The chemical evolution of oligonucleotide therapies of clinical utility, Nat. Biotechnol. 35 (3) (2017) 238–248, https://doi.org/10.1038/nbt.3765.

[12] L. Sandra, H. T'jollyn, N. Goeyvaerts, A. Vermeulen, A.G. Dosne, J.J. Perez-Ruixo, Plasma and liver pharmacokinetics of the N-acetylgalactosamine short interfering RNA JNJ-73763989 in recombinant adeno-associated-hepatitis B virus-infected mice, J. Pharmacol. Exp. Therapeut. 383 (1) (2022) 70–79, https://doi.org/10.1124/jpet.122.001229.

[13] J. Sarvari, Z. Mojtahedi, Y. Kuramitsu, et al., Differential expression of haptoglobin isoforms in chronic active hepatitis, cirrhosis and HCC related to HBV infection, Oncol. Lett. 2 (5) (2011) 871–877, https://doi.org/10.3892/ol.2011.321.

[14] S.T. Cheng, H. Tang, J.H. Ren, X. Chen, A.L. Huang, J. Chen, Interleukin-34 inhibits hepatitis B virus replication in vitro and in vivo, PLoS One 12 (6) (2017) e0179605, https://doi.org/10.1371/journal.pone.0179605.

[15] J.L. Starkey, E.F. Chiari, H.C. Isom, Hepatitis B virus (HBV)-specific short hairpin RNA is capable of reducing the formation of HBV covalently closed circular (CCC) DNA but has no effect on established CCC DNA in vitro, J. Gen. Virol. 90 (Pt 1) (2009) 115–126, https://doi.org/10.1099/vir.0.004408-0.

[16] V.S. Trubetskoy, J.B. Griffin, A.L. Nicholas, et al., Phosphorylation-specific status of RNAi triggers in pharmacokinetic and biodistribution analyses, Nucleic Acids Res. 45 (3) (2017) 1469–1478, https://doi.org/10.1093/nar/gkw828.

[17] R.W. Hui, L.Y. Mak, W.K. Seto, M.F. Yuen, RNA interference as a novel treatment strategy for chronic hepatitis B infection, Clin. Mol. Hepatol. 28 (3) (2022) 408–424, https://doi.org/10.3350/cmh.2022.0012.

[18] T. Schluep, J. Lickliter, J. Hamilton, et al., Safety, tolerability, and pharmacokinetics of ARC-520 injection, an RNA interference-based therapeutic for the treatment of chronic hepatitis B virus infection, in healthy volunteers, Clin. Pharmacol. Drug Dev. 6 (4) (2017) 350–362, https://doi.org/10.1002/cpdd.318.

[19] M.F. Yuen, I. Schiefke, J.H. Yoon, et al., RNA interference therapy with ARC-520 results in prolonged hepatitis B surface antigen response in patients with chronic hepatitis B infection, Hepatology 72 (1) (2020) 19–31, https://doi.org/10.1002/hep.31008.

[20] E. Gane, M.F. Yuen, T.N. Kakuda, et al., JNJ-73763989 pharmacokinetics and safety: liver-targeted siRNAs against hepatitis B virus, in Japanese and non-Japanese healthy adults, and combined with JNJ-56136379 and a nucleos(t)ide analogue in patients with chronic hepatitis B, Antivir. Ther. 27 (3) (2022) 13596535221093856, https://doi.org/10.1177/13596535221093856.

[21] S. Cheng, S.K. Nethi, M. Al-Kofahi, S. Prabha, Pharmacokinetic-pharmacodynamic modeling of tumor targeted drug delivery using nano-engineered mesenchymal stem cells, Pharmaceutics 13 (1) (2021) 92, https://doi.org/10.3390/pharmaceutics13010092.

[22] D. Jean, K. Naik, L. Milligan, et al., Development of best practices in physiologically based pharmacokinetic modeling to support clinical pharmacology regulatory decision-making-A workshop summary, CPT Pharmacometrics Syst. Pharmacol. 10 (11) (2021) 1271–1275, https://doi.org/10.1002/psp4.12706.

[23] J.Y. Jeon, V.S. Ayyar, A. Mitra, Pharmacokinetic and pharmacodynamic modeling of siRNA therapeutics - a minireview, Pharm. Res. (N. Y.) (2022), https://doi.org/10.1007/s11095-022-03333-8.

[24] V.S. Ayyar, D. Song, S. Zheng, T. Carpenter, D.L. Heald, Minimal physiologically based pharmacokinetic-pharmacodynamic (mPBPK-PD) model of N-Acetylgalactosamine-Conjugated small interfering RNA disposition and gene silencing in preclinical species and humans, J. Pharmacol. Exp. Therapeut. 379 (2) (2021) 134–146, https://doi.org/10.1124/jpet.121.000805.

[25] FDA. Givosiran Multi-Discipline Review. https://www.accessdata.fda.gov/drugsatfda_docs/nda/2019/212194Orig1s000MultidisciplineR.pdf.

[26] C. Bon, T. Hofer, A. Bousquet-Mélou, M.R. Davies, B.F. Krippendorff, Capacity limits of asialoglycoprotein receptor-mediated liver targeting, mAbs 9 (8) (2017) 1360–1369, https://doi.org/10.1080/19420862.2017.1373924.

[27] R. Amato, J.F. Gardin, J.A. Tooze, J.M. Cline, Organ weights in relation to age and sex in cynomolgus monkeys (Macaca fascicularis), Toxicol. Pathol. 50 (5) (2022) 574–590, https://doi.org/10.1177/01926233221088283.

[28] D.H. Kim, J.J. Rossi, Strategies for silencing human disease using RNA interference, Nat. Rev. Genet. 8 (3) (2007) 173–184, https://doi.org/10.1038/nrg2006.

[29] C. Xue, S. Hu, Z.H. Gao, et al., Programmably tiling rigidified DNA brick on gold nanoparticle as multi-functional shell for cancer-targeted delivery of siRNAs, Nat. Commun. 12 (1) (2021) 2928, https://doi.org/10.1038/s41467-021-23250-5.

[30] R. McDougall, D. Ramsden, S. Agarwal, et al., The nonclinical disposition and pharmacokinetic/pharmacodynamic properties of N-Acetylgalactosamine-Conjugated small interfering RNA are highly predictable and build confidence in translation to human, Drug Metab. Dispos. 50 (6) (2022) 781–797, https://doi.org/10.1124/dmd.121.000428.

[31] Y. Wang, H. Zhu, R. Madabushi, Q. Liu, S.M. Huang, I. Zineh, Model-informed drug development: current US regulatory practice and future considerations, Clin. Pharmacol. Ther. 105 (4) (2019) 899–911, https://doi.org/10.1002/cpt.1363.

[32] Ranasinghe P, Addison ML, Dear JW, Webb DJ. Small interfering RNA: discovery, pharmacology and clinical development-An introductory review. Br. J. Pharmacol.. doi:10.1111/bph.15972.

[33] C.R. Brown, S. Gupta, J. Qin, et al., Investigating the pharmacodynamic durability of GalNAc-siRNA conjugates, Nucleic Acids Res. 48 (21) (2020) 11827–11844, https://doi.org/10.1093/nar/gkaa670.

[34] S.C. Humphreys, J.A. Davis, S. Iqbal, et al., Considerations and recommendations for assessment of plasma protein binding and drug-drug interactions for siRNA therapeutics, Nucleic Acids Res. 50 (11) (2022) 6020–6037, https://doi.org/10.1093/nar/gkac456.

[35] J.K. Nair, H. Attarwala, A. Sehgal, et al., Impact of enhanced metabolic stability on pharmacokinetics and pharmacodynamics of GalNAc-siRNA conjugates, Nucleic Acids Res. 45 (19) (2017) 10969–10977, https://doi.org/10.1093/nar/gkx818.

[36] W.N. Guo, B. Zhu, L. Ai, D.L. Yang, B.J. Wang, Animal models for the study of hepatitis B virus infection, Zool. Res. 39 (1) (2018) 25–31, https://doi.org/10.24272/j.issn.2095-8137.2018.013.

[37] A.D. Springer, S.F. Dowdy, GalNAc-siRNA conjugates: leading the way for delivery of RNAi therapeutics, Nucleic Acid Therapeut. 28 (3) (2018) 109–118, https://doi.org/10.1089/nat.2018.0736.

[38] J.L.S. Willoughby, A. Chan, A. Sehgal, et al., Evaluation of GalNAc-siRNA conjugate activity in pre-clinical animal models with reduced asialoglycoprotein receptor expression, Mol. Ther. 26 (1) (2018) 105–114, https://doi.org/10.1016/j.ymthe.2017.08.019.

[39] M. Severgnini, J. Sherman, A. Sehgal, et al., A rapid two-step method for isolation of functional primary mouse hepatocytes: cell characterization and asialoglycoprotein receptor based assay development, Cytotechnology 64 (2) (2012) 187–195, https://doi.org/10.1007/s10616-011-9407-0.

[40] R. Kanasty, J.R. Dorkin, A. Vegas, D. Anderson, Delivery materials for siRNA therapeutics, Nat. Mater. 12 (11) (2013) 967–977, https://doi.org/10.1038/nmat3765.

[41] V. Goel, N.H. Gosselin, C. Jomphe, X. Zhang, J.F. Marier, G.J. Robbie, Population pharmacokinetic-pharmacodynamic model of serum transthyretin following patisiran administration, Nucleic Acid Therapeut. 30 (3) (2020) 143–152, https://doi.org/10.1089/nat.2019.0841.

[42] A. Boianelli, Y. Aoki, M. Ivanov, A. Dahlén, P. Gennemark, Cross-species translation of biophase half-life and potency of GalNAc-conjugated siRNAs, Nucleic Acid Therapeut. 32 (6) (2022) 507–512, https://doi.org/10.1089/nat.2022.0010.

[43] B. Pasquiers, S. Benamara, M. Felices, L. Nguyen, X. Declèves, Review of the existing translational pharmacokinetics modeling approaches specific to monoclonal antibodies (mAbs) to support the first-in-human (FIH) dose selection, Int. J. Mol. Sci. 23 (21) (2022) 12754, https://doi.org/10.3390/ijms232112754.

[44] Q. Huang, J.E. Riviere, The application of allometric scaling principles to predict pharmacokinetic parameters across species, Expet Opin. Drug Metab. Toxicol. 10 (9) (2014) 1241–1253, https://doi.org/10.1517/17425255.2014.934671.